Natural Boundary Transition and Inherent Dynamic Control of a Hybrid-Mode-Modulated Dual-Active-Bridge Converter

Jingxin Hu, *Member, IEEE*, Shenghui Cui, *Member, IEEE*, and Rik W. De Doncker, *Fellow, IEEE*

***Abstract*—This article proposes a hybrid-mode modulation strategy for the single-phase dual-active-bridge (DAB) dc–dc converter that realizes soft switching in the whole operating range. Different from existing modulation methods that are usually dependent on complex mathematical optimization processes, the presented article reveals that the simple trapezoidal continuous conduction mode and triangular discontinuous conduction mode inspired by a quasi-single-active-bridge operation can naturally and sequentially extend the soft-switching boundary of the conventional single-phase-shift (SPS) modulation to the full range in both the buck and boost modes. Meanwhile, the transformer rms current is also reduced. Moreover, a fast-dynamic control with inherent seamless mode transitions is realized by introducing the predictive-current SPS modulation. The proposed hybrid-mode modulation strategy with closed-form solutions can be easily implemented in a generalized closed-loop controller, which enables an ultrawide-voltage-range operation of the DAB converter with significantly elevated efficiency and fast transient responses. The effectiveness of the proposed method is validated by comprehensive experimental results from a small-scale DAB prototype.**

***Index Terms*—Dual-active-bridge (DAB), dynamic control, modulation schemes, single-active-bridge (SAB), smooth transition, soft switching, wide operating voltage range.**

I. Introduction

THE dual-active-bridge (DAB), first proposed in 1988 for aerospace applications [1], [2], is one of the most popular bidirectional isolated dc–dc converter topologies. Due to its attractive features such as inherent soft-switching capability, buck and boost operation, and high power density, it is ideal for dc solid-state transformers in grid applications [3]–[6], renewable energy integration [7], [8], energy storage systems [9], as well as more-electric transportation systems [10]–[13].

The single-phase-shift (SPS) is the original, and meanwhile, the simplest modulation method for the DAB converter [2]. With adequate inductive reactive currents in the high-frequency ac-link transformer, all power semiconductor devices can realize zero-voltage switching (ZVS), which leads to high-efficiency operation and clean switching waveforms with low electromagnetic interference (EMI). However, when the output-to-input voltage ratio deviates greatly from unity especially under light-load conditions, the DAB converter will not only lose soft switching but also suffer from high rms current. Thus, despite its advantages under the nominal operating condition, the SPS modulation is not sufficient to guarantee high-efficiency operation of the DAB converter in the full operating range.

To address this issue, several alternative modulation schemes with adjustable duty ratios of the input and output ac voltages have been proposed in the literature, which are comprehensively summarized in [14]. In [15] and [16], the extended-phase-shift (EPS) modulation is proposed, which can realize soft switching in the full operating range. However, the EPS modulation still suffers from a relatively high rms current under light-load conditions. Moreover, due to lack of closed-form solutions, the EPS modulation usually has to be implemented in lookup-tables, which has considerable constraints in practical applications. To improve the applicability of this method, the fundamental-optimal strategy (FOPS) is proposed in [17], which can be implemented in a unified controller with simple calculations. However, the maximum power transfer capability and the soft-switching range are compromised. In [18], the dual-phase-shift (DPS) modulation is proposed to eliminate the reactive power and boost the system efficiency. Unfortunately, it cannot realize full-range soft-switching. Besides, similar to the EPS, the DPS modulation also lacks a closed-form solution to its control variables. The triple-phase-shift (TPS) modulation presented in [19] and [20] inherently provides sufficient degrees of freedom to extend the soft-switching range and meanwhile reduce the rms current. However, it consists of many possible switching modes that complicates the parameter determination. The optimal switching pattern and control variables of the TPS modulation are normally derived from the complex mathematical optimization process [21]–[25]. This usually results in a

Manuscript received June 1, 2021; revised August 27, 2021; accepted October 10, 2021. Date of publication October 14, 2021; date of current version December 31, 2021. This work was supported in part by European Union's Horizon 2020 Research and Innovation Programme under Grant 957788 - Project HYPERRIDE, and in part by the Federal Ministry of Education and Research (BMBF, FKZ03SF0490), Flexible Electrical Networks (FEN) Research Campus. Recommended for publication by Associate Editor J. Biela. *(Corresponding author: Shenghui Cui.)*

Jingxin Hu and Rik W. De Doncker are with the Institute for Power Generation and Storage Systems, E.ON ERC and FEN Research Campus, RWTH Aachen University, 52074 Aachen, Germany (e-mail: jhu@eonerc.rwth-aachen.de; post_pgs@eonerc.rwth-aachen.de).

Shenghui Cui is with the Department of Electrical and Computer Engineering, Seoul National University, Seoul 08826, South Korea (e-mail: cuish@snu.ac.kr).

Color versions of one or more figures in this article are available at https://doi.org/10.1109/TPEL.2021.3119903.

Digital Object Identifier 10.1109/TPEL.2021.3119903

hybrid-mode operation, which is not intuitive due to lack of physical insights in the circuit. Moreover, modulation-mode transitions under transient operation conditions can induce a transient dc-bias current in the high-frequency ac-link transformer. This can highly degrade the dynamic performance of the converter or even cause the transformer core saturation. Although the transient dc bias can be suppressed by dedicated control methods [26]–[30], this usually requires sophisticated gating logic and increases the computational complexity of the hybrid-mode operation.

Distinguished from the aforementioned methods, this article proposes a hybrid-mode modulation strategy that is inspired by the quasi-single-active-bridge operation. The analysis first reveals that the ZVS boundary of the SPS modulation in the buck mode can be naturally and sequentially extended to the full operating range by the continuous and discontinuous conduction modes of the single-active-bridge (SAB) converter. The switching patterns of the DAB converter are then designed to emulate the operation waveforms of the SAB converter in both buck and boost modes, respectively, which can cover the whole hard-switching region of the SPS modulation with soft-switching and reduced rms current. The resulting hybrid-mode modulation not only has a natural boundary transition, but also benefits from closed-form solutions, which enables simple model-based control implementation. Moreover, with the predictive-current SPS modulation, the proposed hybrid-mode modulation can realize inherent dynamic control and smooth mode transitions without transient dc-bias current. Notice that the fast-dynamic control does not require any additional gating logic under transient operation conditions, which minimizes the complexity of the control algorithm. Thus, with the proposed method, the DAB converter can operate in an ultrawide voltage range with both a high efficiency and a fast transient response.

It is worth mentioning that the motivation of this article is not to provide another globally optimized modulation method for the DAB converter, but to reveal a simple and intuitive hybrid-mode modulation method based on the intrinsic circuit behaviors. Notice that it is also possible to emulate the operation of an asymmetrical-dual-active-bridge (ADAB) [31], [32], also known as semi-dual-active-bridge (SDAB) [33], which has more control freedoms to optimize the performance than the SAB converter. However, due to multiple control variables, the ADAB converter still requires a complex optimization procedure for modulation schemes and dedicated dynamic control methods to suppress transient dc-bias currents. Therefore, the ADAB operation is not considered in this article.

The rest of the article is organized as follows. First, the proposed hybrid-mode modulation schemes, are introduced in Section II with their origin from the SAB operation and the corresponding closed-form solutions. This is followed by a description of the inherent dynamic control and the implementation of the unified voltage control in Section III. Furthermore, in Section IV, the proposed modulation and control methods are verified by comprehensive experimental results from a small-scale laboratory prototype. Finally, Section V concludes this article.

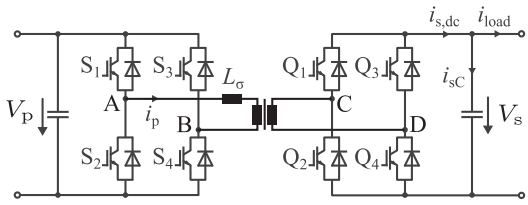

Fig. 1. Circuit diagram of the single-phase DAB converter.

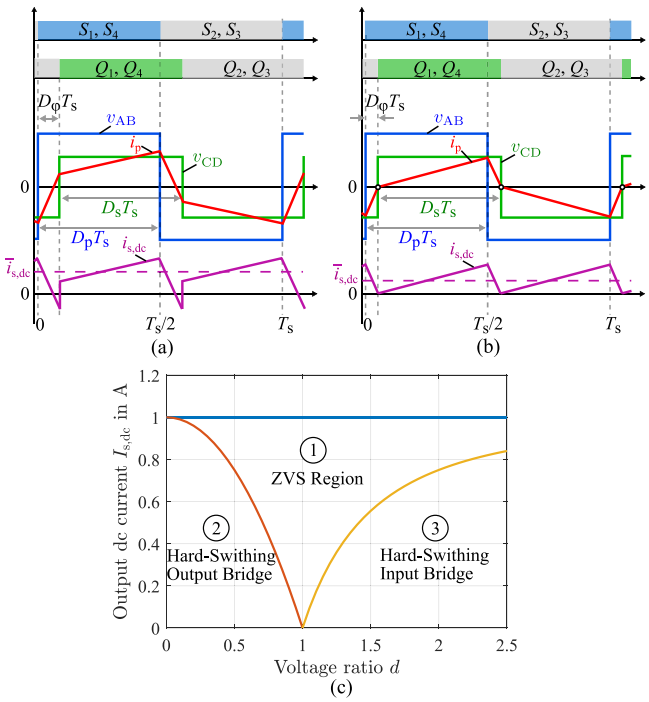

Fig. 2. Key operation waveforms and characteristics of the SPS modulation. (a) Typical ZVS operation waveforms. (b) Operation waveforms at the ZVS boundary in the buck mode. (c) ZVS region.

II. Modulation Schemes

The single-phase DAB converter consists of two H-bridges linked by a high-frequency ac transformer, as depicted in Fig. 1. The total leakage inductance L_σ is employed as the energy transfer element, whose current is driven by the difference between the ac voltages of the input and output bridges, i.e. $v_{\rm AB}$ and $v_{\rm CD}$, respectively. The DAB converter normally has three control variables, which are the duty ratios $D_{\rm p}$ and $D_{\rm s}$ of the input and output ac voltages, respectively, and the phase-shift ratio D_φ between two bridges.

A. Single-Phase-Shift Modulation and Its ZVS Boundary

As the original method, the SPS modulation is still one of the most commonly used operation schemes for the DAB converter due to its simplicity. As shown in Fig. 2(a), in the SPS modulation, $D_{\rm p}$ and $D_{\rm s}$ are fixed to 0.5, and only D_φ is employed as the control variable to change the power flow. For sake of simplicity, only the positive power flow is hereinafter considered. The transformer current $i_{\rm p}$ can be expressed by

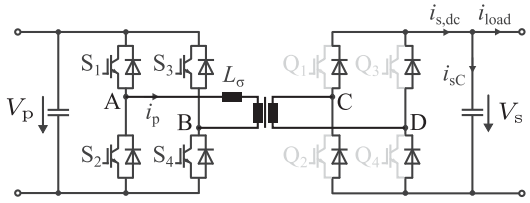

Fig. 3. Circuit diagram of the single-phase SAB converter.

piecewise linear functions [2], whereby the averaged output dc current I_{s-dc} and its maximum value are calculated as

$$I_{s,dc} = \frac{N_{tr} V_p D_\varphi (1 - 2D_\varphi)}{f L_\sigma} \tag{1}$$

$$I_{s,dc,max} = \frac{N_{tr} V_p}{8 f L_\sigma}, \quad \text{at } D_\varphi = 0.25 \tag{2}$$

where N_{tr} denotes the turns ratio of the transformer, V_p denotes the input dc voltage, and f denotes the switching frequency.

According to (1), in the SPS modulation, $I_{s,dc}$ is independent of the output dc voltage V_s. Furthermore, D_φ is calculated by

$$D_\varphi = \frac{1}{4} \cdot \left(1 - \sqrt{1 - \frac{8 f L_\sigma I_{s,dc}}{N_{tr} V_p}} \right). \tag{3}$$

When the transformer current flows into the antiparallel diodes at the turn-ON instant of the corresponding switch, ZVS turn-ON is realized. This leads to the soft-switching condition

$$\begin{cases} i_p(0) = \frac{(d-1-4dD_\varphi)V_p}{4fL_\sigma} \le 0, & \text{for input bridge} \\ i_p(D_\varphi T_s) = \frac{(4D_\varphi - 1 + d)V_p}{4fL_\sigma} \ge 0, & \text{for output bridge} \end{cases} \tag{4}$$

where $d = {}^{N_{tr} V_s}/_{V_p}$ denotes the dc voltage ratio, and $T_s = {}^1/_f$ denotes the switching period.

Fig. 2(b) depicts the operation waveforms under the ZVS-boundary condition of the SPS modulation in the buck mode ($d < 1$), where the switches in the output bridge realize zero-current-switching (ZCS) turn-OFF. Substituting (4) into (1), the ZVS boundary of the SPS modulation can be identified in (5), which is also shown in Fig. 2(c). It can be observed that, in the SPS modulation, the DAB converter realizes soft switching when the voltage ratio is close to unity and the load current is relatively high. Moreover, the hard-switching regions of the output bridge and the input bridge are located in the buck mode ($d < 1$) and the boost mode ($d > 1$), respectively.

$$\begin{cases} I_{s,dc} \ge \frac{N_{tr} V_p (d^2 - 1)}{8 f L_\sigma d^2}, & \text{for input bridge} \\ I_{s,dc} \ge \frac{N_{tr} V_p (1 - d^2)}{8 f L_\sigma}, & \text{for output bridge.} \end{cases} \tag{5}$$

B. Operation Boundary of an SAB Converter

When the gating signals of the switches in the output bridge are disabled, the output bridge operates as a diode rectifier. The circuit topology effectively turns into a single-phase SAB converter as depicted in Fig. 3. The SAB is a unidirectional isolated buck-type dc–dc converter, which regulates the power flow by adjusting the duty ratio D_p of the input ac voltage [2].

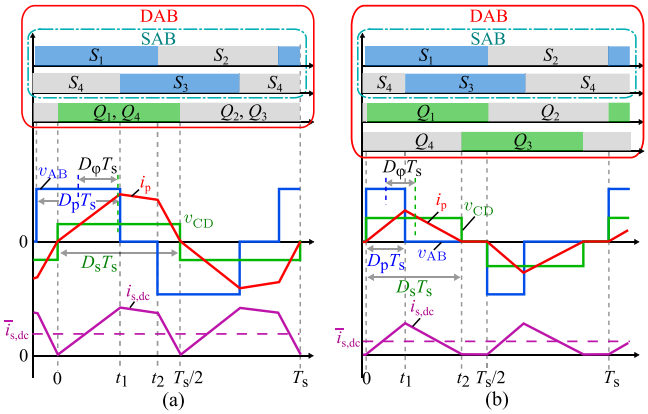

Fig. 4. Key operation waveforms of the SAB converter and the quasi-SAB operation in the buck mode. (a) Trapezoidal continuous conduction mode (buck). (b) Triangular discontinuous conduction mode (buck).

Due to the existence of the output diode rectifier, the transformer current is always in phase with the output ac voltage, which leads to the ZCS turn-OFF of the diode rectifier. Dependent on the load condition, the SAB converter can operate in either the continuous conduction mode (CCM) or the discontinuous conduction mode (DCM) [34]–[36], which are described in detail as follows. Since the output bridge is not switched in the SAB converter, the variables D_φ and D_s in Section II-B represent the equivalent external and internal phase-shift ratios judged from the voltage waveforms of the SAB converter.

1) CCM: The SAB converter operates in the CCM at a relatively high load current. As depicted in Fig. 4(a), the input ac voltage v_{AB} leads the output ac voltage v_{CD} with an equivalent phase-shift ratio $D_\varphi \ge 0$. The transformer current is continuous with a trapezoidal waveform. Therefore, it is hereinafter named as trapezoidal CCM (TZ-CCM-Buck). In the TZ-CCM-Buck mode, the equivalent duty ratio D_s of the output bridge is always 0.5. The input bridge can realize ZVS turn-ON, while the output bridge can realize ZCS turn-OFF. Therefore, hard switching with a diode reverse recovery is avoided under this condition.

The transformer current of the TZ-CCM-Buck mode can also be expressed by piecewise linear functions [2]. The expression of D_φ is given by

$$D_\varphi = \frac{1 - d}{4} \tag{6}$$

which is only related to the voltage ratio d.

The relationship between $I_{s,dc}$ and D_p is described as

$$I_{s,dc} = \frac{N_{tr} V_p (-4D_p^2 + 4D_p - d^2)}{8 f L_\sigma}. \tag{7}$$

Thereby, D_p is calculated as

$$D_p = \frac{1}{2} - \sqrt{\frac{1 - d^2}{4} - \frac{2 f L_\sigma I_{s,dc}}{N_{tr} V_p}}. \tag{8}$$

For a given voltage ratio d, the maximum output dc current is obtained at $D_p = 0.5$, while the minimum output dc current is obtained at $D_p = \frac{d}{2}$. Therefore, the upper and lower boundaries

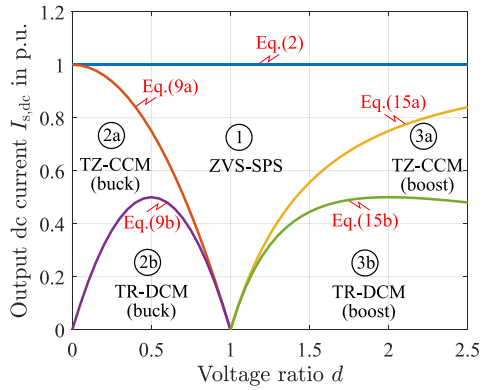

Fig. 5. Operation range of the proposed hybrid-mode modulation.

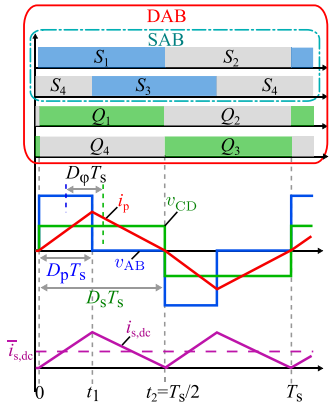

Fig. 6. Operation waveforms of the boundary condition between the TZ-CCM-Buck and TR-DCM-Buck modes.

of the TZ-CCM-Buck mode are defined as

$$I_{\mathrm{s,dc,max}} = \frac{N_{\mathrm{tr}} V_{\mathrm{p}} (1-d^2)}{8 f L_\sigma} \tag{9a}$$

$$I_{\mathrm{s,dc,min}} = \frac{N_{\mathrm{tr}} V_{\mathrm{p}} d(1-d)}{4 f L_\sigma} \tag{9b}$$

which are plotted in Fig. 5. Comparing (5) and (9a), one can easily identify that the upper boundary of the TZ-CCM-Buck mode is also the ZVS boundary of the SPS modulation in the buck mode, where the operation waveforms of two modes are identical as shown in Fig. 2(b).

2) DCM: The SAB converter operates in the DCM at a lower load current. The transformer current is discontinuous with a triangular waveform, as depicted in Fig. 4(b). Therefore, it is hereinafter named as triangular DCM (TR-DCM-Buck). In the TR-DCM-Buck mode, D_{s} changes with D_{p} according to $D_{\mathrm{s}} = \frac{D_{\mathrm{p}}}{d}$. D_φ is defined as $D_\varphi = \frac{D_{\mathrm{s}} - D_{\mathrm{p}}}{2} = \frac{D_{\mathrm{s}}(1-d)}{2}$. As shown in Fig. 4(b), half of the switches in the input bridge can realize ZVS turn-ON, and the other half can realize ZCS turn-OFF as the output bridge. Therefore, no hard-switching operation with a diode reverse recovery occurs under this condition.

The average output dc current with its maximum and minimum values is given by

$$I_{\mathrm{s,dc}} = \frac{4 N_{\mathrm{tr}} V_{\mathrm{p}} d D_\varphi^2}{(1-d) f L_\sigma} \tag{10}$$

$$I_{\mathrm{s,dc,max}} = \frac{N_{\mathrm{tr}} V_{\mathrm{p}} d(1-d)}{4 f L_\sigma}, \qquad \text{at } D_\varphi = \frac{1-d}{4} \tag{11a}$$

$$I_{\mathrm{s,dc,min}} = 0, \qquad \text{at } D_\varphi = 0. \tag{11b}$$

From (10), D_φ is calculated as

$$D_\varphi = \sqrt{\frac{(1-d) f L_\sigma I_{\mathrm{s,dc}}}{4 d N_{\mathrm{tr}} V_{\mathrm{p}}}}. \tag{12}$$

The operation range of the TR-DCM-Buck mode is depicted in Fig. 5, which has a natural boundary transition from the TZ-CCM-Buck mode. Fig. 6 further shows the operation waveforms under the boundary condition. Therefore, with a combination of the TZ-CCM-Buck, TR-DCM-Buck, and SPS modulation modes, as depicted in Fig. 5, the DAB converter can realize full-range soft switching in the buck mode.

Although the SAB operation can extend the soft-switching range of the DAB converter, it also has several constraints, which are as follows.

1) In the TR-DCM-Buck mode, the operation state of the output diode rectifier is undefined in the zero-current interval, which will result in a high-frequency oscillation of v_{CD} due to parasitics in the circuit. This can potentially cause EMI issues.

2) If unipolar transistors, e.g., MOSFETs, are employed, the SAB operation cannot take the advantage of the synchronous rectification to reduce the conduction loss in the output bridge.

3) Most importantly, the SAB operation is only valid in the buck mode.

C. Proposed Hybrid-Mode Modulation With Natural Boundary Transition

To tackle these issues, a hybrid-mode modulation is proposed for the DAB converter to imitate the SAB operation in the whole hard-switching region of the SPS modulation.

1) TZ-CCM-Buck and TR-DCM-Buck: In the buck mode, the same TZ-CCM-Buck and TR-DCM-Buck modes are employed except for applying the synchronous rectification technique. As shown in Fig. 4, according to the derived closed-form solutions in Section II-B, the devices in the output bridge are switched to generate exactly the same ac voltage waveform as the SAB converter in these two modes. Thus, the output bridge can not only maintain ZCS turn-OFF, but also reduce the conduction loss due to lower ON-state voltage of MOSFETs than the forward voltage of diodes. Moreover, since a zero-voltage state is defined for v_{CD} in the zero-current interval in the TR-DCM-Buck mode, the EMI issue due to an oscillating ac voltage can be avoided. It should be also noticed that the TZ-CCM-Buck and TR-DCM-Buck modes are effectively special conditions of the EPS modulation and the TPS modulation, respectively.

2) TZ-CCM-Boost and TR-DCM-Boost: To achieve the similar operation performance in the boost mode, the TZ-CCM-Buck and TR-DCM-Buck modes are mirrored and modified to the

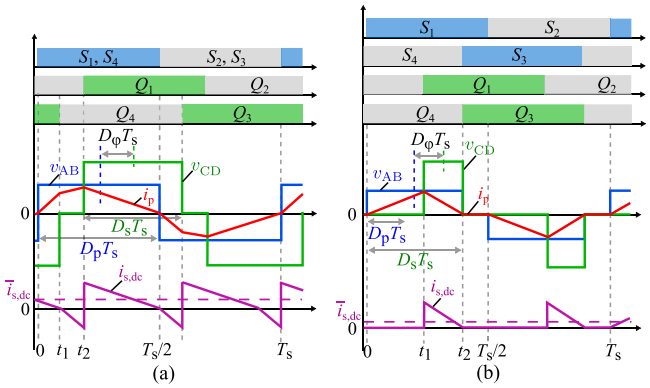

Fig. 7. Key operation waveforms in the boost mode. (a) Trapezoidal continuous conduction mode (boost). (b) Triangular discontinuous conduction mode (boost).

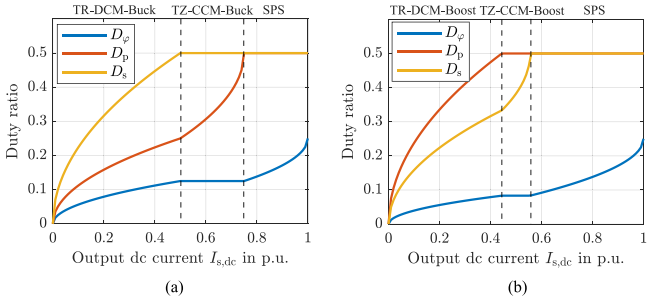

Fig. 8. Control variables D_φ, D_p, and D_s of the proposed modulation method at a variable output dc current. (a) At $d = 0.5$. (b) At $d = 1.5$.

TZ-CCM-Boost and TR-DCM-Boost modes, respectively, as depicted in Fig. 7.

As shown in Fig. 7(a), the TZ-CCM-Boost mode maintains a continuous trapezoidal current waveform. However, as a mirrored version of the TZ-CCM-Buck mode, D_p is fixed to 0.5, while D_s along with D_φ is adapted to realize ZCS turn-OFF of the switches in the input bridge. Meanwhile, the output bridge can realize ZVS turn-ON. The transformer current can be similarly expressed in piecewise linear functions. The ZCS turn-OFF condition of $i_p(0) = i_p(\frac{T_s}{2}) = 0$ yields

$$D_\varphi = \frac{d-1}{4d}. \tag{13}$$

The averaged output dc current with its maximum and minimum values of the TZ-CCM-Boost mode is given by

$$I_{s,dc} = \frac{N_{tr}V_p(-4d^2D_s^2 + 4d^2D_s - 1)}{8d^2fL_\sigma} \tag{14}$$

$$I_{s,dc,max} = \frac{N_{tr}V_p(d^2-1)}{8d^2fL_\sigma}, \qquad \text{at } D_s = \frac{1}{2} \tag{15a}$$

$$I_{s,dc,min} = \frac{N_{tr}V_p(d-1)}{4d^2fL_\sigma}, \qquad \text{at } D_s = \frac{1}{2d}. \tag{15b}$$

From (14), D_s in the TZ-CCM-Boost mode is obtained by

$$D_s = \frac{1}{2} - \sqrt{\frac{d^2-1}{4d^2} - \frac{2fL_\sigma I_{s,dc}}{N_{tr}V_p}}. \tag{16}$$

According to (15a) and (15b), the operation region of the TZ-CCM-Boost mode is depicted in Fig. 5, which transits naturally from the ZVS boundary of the SPS modulation.

The last remaining piece of the hard-switching region in Fig. 5 is finally covered by the TR-DCM-Boost mode, which is derived by mirroring the switching pattern of the TR-DCM-Buck mode as depicted in Fig. 7(b). To realize the desired discontinuous triangular current waveform, $D_p = dD_s$ needs to be maintained. Thus, D_φ is defined as $D_\varphi = \frac{(d-1)D_s}{2}$. In this mode, half of the switches in the output bridge can realize ZVS turn-ON, while the remaining switches in both the input and output bridges can realize ZCS turn-OFF.

TABLE I
EXPRESSIONS OF THE TRANSFORMER RMS CURRENT IN DIFFERENT MODULATION MODES

Mode	Expression of $I_{p,rms}$
SPS	$\frac{\sqrt{3}N_{tr}V_p}{12fL_\sigma}\sqrt{-64dD_\varphi^3 + 48dD_\varphi^2 + (d-1)^2}$
TZ-CCM-Buck	$\frac{\sqrt{3}N_{tr}V_p}{6fL_\sigma}\sqrt{-\frac{(2D_p-d)^3}{2} + (d-1)^2(\frac{3(2D_p-d)^2}{4} + \frac{3(2D_p-d)}{2} + d^2)}$
TR-DCM-Buck	$\frac{4N_{tr}V_pdD_\varphi}{fL_\sigma}\sqrt{\frac{D_\varphi}{3(1-d)}}$
TZ-CCM-Boost	$\frac{\sqrt{3}N_{tr}V_p}{6dfL_\sigma}\sqrt{-\frac{d(2dD_s-1)^3}{2} + (d-1)^2(\frac{3(2dD_s-1)^2}{4} + \frac{3(2dD_s-1)}{2} + 1)}$
TR-DCM-Boost	$\frac{4N_{tr}V_pD_\varphi}{fL_\sigma}\sqrt{\frac{dD_\varphi}{3(d-1)}}$

The averaged output dc current with its maximum and minimum values of the TR-DCM-Boost mode is given by

$$I_{s,dc} = \frac{4N_{tr}V_pD_\varphi^2}{(d-1)fL_\sigma} \tag{17}$$

$$I_{s,dc,max} = \frac{N_{tr}V_p(d-1)}{4fL_\sigma d^2}, \qquad \text{at } D_\varphi = \frac{d-1}{4d} \tag{18a}$$

$$I_{s,dc,min} = 0, \qquad \text{at } D_\varphi = 0. \tag{18b}$$

From (10), D_φ in the TR-DCM-Boost mode is obtained by

$$D_\varphi = \sqrt{\frac{(d-1)fL_\sigma I_{s,dc}}{4N_{tr}V_p}}. \tag{19}$$

The operation region of the TR-DCM-Boost mode is depicted in Fig. 5, which further extends the soft-switching range toward no-load conditions with a natural boundary transition from the TZ-CCM-Boost mode.

Therefore, combining the SPS, TZ-CCM-Buck, TR-DCM-Buck, TZ-CCM-Boost, and TR-DCM-Boost modes, the DAB converter can realize full-range soft-switching with seamless mode transitions. It is worth mentioning that the natural boundary transition is not only for the output dc current, but also for control variables in the switching patterns as depicted in Fig. 8. It is shown that in both the buck and boost modes the control variables, i.e., D_φ, D_p, and D_s, change continuously between two adjacent modulation modes. Moreover, according to the derived expressions of the rms current for these modulation modes as given in Table I, the large rms current in the hard-switching region of the SPS modulation is significantly reduced by the proposed hybrid-mode modulation method, as depicted in Fig. 9.

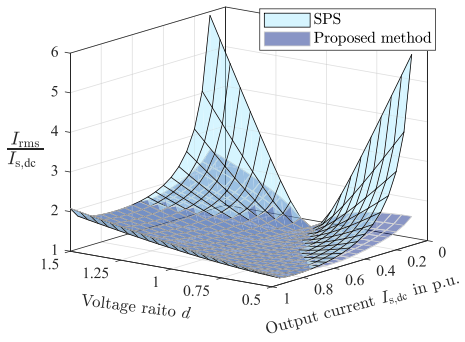

Fig. 9. Ratio between the rms current and the output dc current in the whole operating range.

III. Inherent Dynamic Control

When the DAB converter operates under transient conditions, the switching pattern along with its control variables D_p, D_s, and D_φ can dynamically change, which leads to either a state change in the same modulation mode or a mode transition. When the initial steady-state currents of two consecutive switching patterns are different, a transient dc-bias is induced in the transformer current. This can result in degraded transient performance or even cause transformer core saturation. Therefore, the dynamic current control is necessary for the hybrid-mode operation of the DAB converter.

The aforementioned CCM and DCM in both the buck and boost modes have a common feature, which is ZCS turn-OFF of the switches. Therefore, it is convenient to align the starting instant of the switching pattern with a ZCS turn-OFF instant in each switching cycle. Specifically, the starting instant of the switching period in both the TZ-CCM-Buck and TR-DCM-Buck modes is aligned with the rising edge of the positive v_{CD} at $i_p = 0$, as depicted in Fig. 4. For the TZ-CCM-Boost and TR-DCM-Boost modes, the starting instant of the switching pattern is aligned with the rising edge of the positive v_{AB} at $i_p = 0$, as depicted in Fig. 7. Thereby, the initial and ending steady-state currents in these modulation modes are always zero, which inherently avoids a transient dc-bias current.

A. Predictive-Current Single-Phase-Shift for Smooth Mode Transitions

Different from the CCM and DCM modes, the SPS modulation usually does not have a ZCS turn-OFF instant of switches except for the ZVS boundary condition. To enable a smooth mode transition without a transient dc-bias current, the starting instant of the switching pattern needs to be determined by predicting the zero crossing of the transformer current. Fortunately, as depicted in Fig. 10(a), the zero crossing of i_p is always in the phase-shift interval between the rising edges of v_{AB} and v_{CD}, since only the ZVS region of the SPS modulation is considered in the proposed method. Based on the derived expression of the piecewise linear current [2], the time interval t_x between the rising edge of v_{AB} and the current zero crossing can be calculated by

$$t_x = \frac{4dD_\varphi + 1 - d}{4(1+d)f}. \tag{20}$$

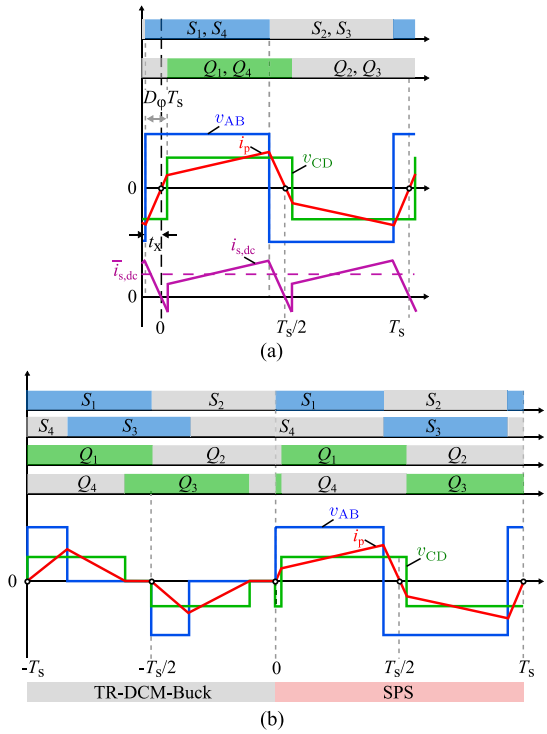

Fig. 10. Key operation waveforms of the inherent dynamic control. (a) Predictive-current SPS modulation. (b) Mode transition from the TR-DCM-Buck to the predictive-current SPS modulation.

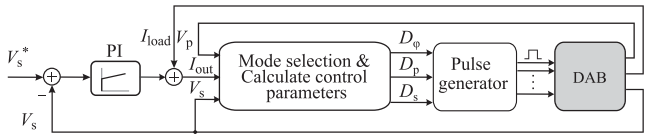

Fig. 11. Generalized closed-loop control block diagram for the DAB converter.

By delaying the starting instant of the switching pattern with a time interval of t_x from the rising edge of v_{AB}, the initial and ending steady-state currents of the SPS modulation are also zero, as depicted in Fig. 10(a). Thus, the DAB converter can inherently realize a dynamic current control and smooth mode transitions as shown in Fig. 10(b). Compared with other methods that suppress the induced transient dc-bias current [26]–[30], the proposed modulation methods inherently avoids this issue, which improves the transient performance with minimized computational efforts.

B. Unified Hybrid-Mode Voltage Control

The proposed hybrid-mode modulation strategy can be implemented in a generalized closed-loop voltage controller, as depicted in Fig. 11. The output dc voltage is simply controlled by a proportional–integral (PI) regulator, which generates a reference output dc current. With the derived closed-form solutions for the modulation modes in Section II, a model-based feed-forward function is constructed, which selects the suitable modulation mode and directly calculates the corresponding control variables based on the measured dc voltage ratio and reference output

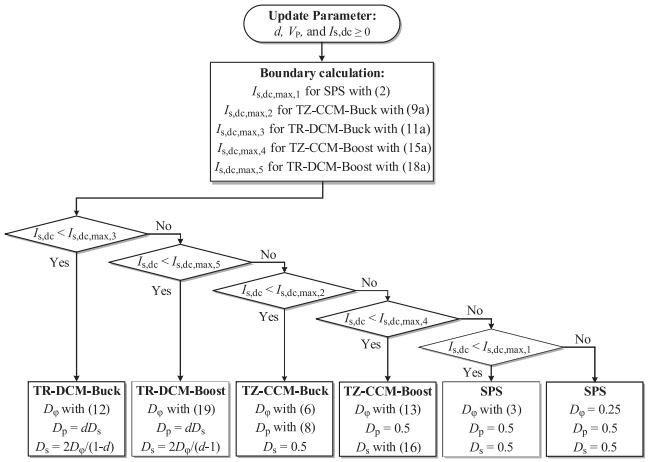

Fig. 12. Flowchart of the model-based feed-forward function.

dc current. Such kind of model-based feed-forward control is beneficial to improve the dynamic performance of the DAB converter [37]. Fig. 12 presents the flowchart of the model-based feed-forward function. As depicted in Fig. 11, the feed-forward path of I_{load} can be implemented to constitute the reference output dc current together with the output of the voltage PI regulator. Thereby, the closed-loop control has a better capability of rejecting the load disturbance, leading to a faster load transient response. Notice that the steady-state switching pattern of each mode is precalculated with zero initial current as illustrated in Section III-A, a dedicated dynamic controller to calculate the transient switching pattern is no longer required.

C. Discussion on Parameter Tolerance and Nonlinearities

As the proposed current control is based on feed-forward functions, the parameter tolerance particularly in the inductance value can influence the operation of the DAB converter. Take the TR-DCM-Buck mode as an example, the phase-shift ratio $D_{\varphi,\mathrm{calc}}$ is calculated based on the reference output dc current $I_{\mathrm{s,dc,ref}}$ and the leakage inductance L_σ according to

$$D_{\varphi,\mathrm{calc}} = \sqrt{\frac{(1-d)fL_\sigma I_{\mathrm{s,dc,ref}}}{4dN_{\mathrm{tr}}V_{\mathrm{p}}}}. \tag{21}$$

Assuming the actual leakage inductance is $L_{\sigma,\mathrm{actual}} = k \cdot L_\sigma$ with a scaling factor k, it yields to an actual output dc current by substituting (21) into (10)

$$I_{\mathrm{s,dc,actual}} = \frac{4N_{\mathrm{tr}}V_{\mathrm{p}}dD_{\varphi,\mathrm{calc}}^2}{(1-d)fL_{\sigma,\mathrm{actual}}} = \frac{I_{\mathrm{s,dc,ref}}}{k} \tag{22}$$

which is scaled by $1/k$ compared with the reference value.

This introduces an error of $(1-1/k)I_{\mathrm{s,dc,ref}}$ in the output dc current. Due to the existence of the voltage PI regulator in the controller as shown in Fig. 11, the reference output dc current $I_{\mathrm{s,dc,ref}}$ will be adapted to compensate the error caused by the leakage inductance. Therefore, the dynamic response of the DAB converter will be clearly slower with a tolerance in the leakage inductance, as shown in the simulation result in Fig. 13(a). However, since the relationships of control variables D_φ, D_{p}, and D_{s} are independent from the leakage inductance

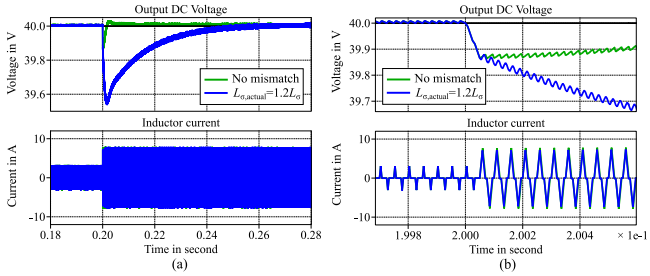

Fig. 13. Simulation results of a load step response with the proposed control method considering tolerance in the leakage inductance. Simulation parameters are $V_{\mathrm{p}} = 80\,\mathrm{V}$, $V_{\mathrm{s}} = 40\,\mathrm{V}$, $N_{\mathrm{tr}} = 1$, $f = 20\,\mathrm{kHz}$, $L_\sigma = 39\,\mu\mathrm{H}$, output capacitance $C_{\mathrm{out}} = 1\,\mathrm{mF}$, proportional gain $K_{\mathrm{P}} = 0.83$, and integral gain $K_{\mathrm{I}} = 34.74$. (a) Full-time view. (b) Zoom-in view.

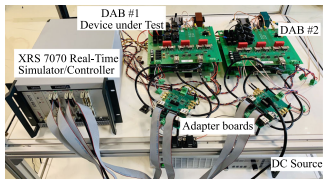

Fig. 14. Schematic diagram of the experimental setup.

in the proposed method, the triangular inductor current with ZCS turn-OFF can still be realized even with a tolerance in the leakage inductance, as shown in Fig. 13(b). Moreover, it is worth mentioning that the accurate parameter of the leakage inductance in the DAB converter can be identified online using the method proposed in [38]. Thereby, the model parameter can be continuously updated to improve the dynamic response of the DAB converter.

It should be also mentioned that the nonlinearities such as dead time and parasitic capacitance have some impacts on the instant current calculations, which can be addressed with dedicated methods. In [39], the dead time can be effectively compensated in the triangular and trapezoidal modulation to mitigate the distortion effect. The parasitic capacitance can be compensated by the charge-based modulation as proposed in [40], which, however, inevitably increases the computational efforts. Another possible approach is to compensate the nonlinear effects in the trapezoidal and triangular modulation by empirically correcting the switching timings according to [41], which requires parameter tuning through experiments.

IV. Experimental Verification

A small-scale DAB converter prototype, as shown in Fig. 14, is built to verify the proposed modulation and control methods. Detailed parameters of the prototype are given in Table II. A second DAB converter with the same specifications is employed to circulate the power in the experiments. The input voltage is always fixed to 80 V. An XRS 7070 real-time controller from AixControl is employed for the experimental implementation, which is internally based on a DSP+FPGA architecture. Considering the simple switching patterns and the fair computational complexity, the proposed control can also be easily implemented on other control platforms such as commercial DSPs or FPGAs with DSP slices.

TABLE II
EXPERIMENTAL PARAMETERS

Parameter	Value
Input dc voltage	80 V
Total leakage inductance	39 μH
Transformer turns ratio	1:1
Switching frequency	20 kHz
Output capacitance	1 mF
Dead time	1.0 μs

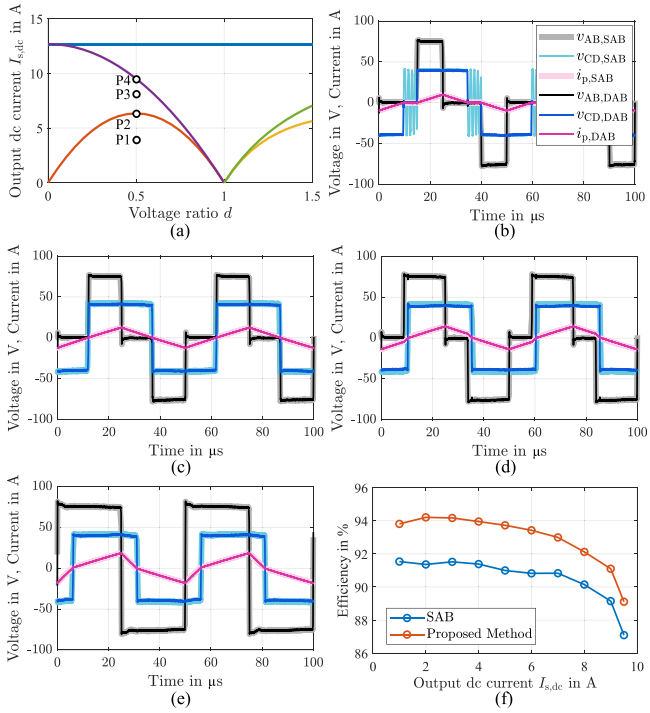

Fig. 15. Comparison of the SAB operation and the proposed hybrid-mode modulation. (a) Operation boundary of the DAB prototype. (b) Experimental waveforms of the TR-DCM-Buck mode at point P1. (c) Experimental waveforms of the boundary condition between TR-DCM-Buck and TZ-CCM-Buck at point P2. (d) Experimental waveforms of the TZ-CCM-Buck mode at point P3. (e) Experimental waveforms of the boundary condition between TR-CCM-Buck and SPS at point P4. (f) Measured efficiency curves at $d = 0.5$.

A. Comparison With the SAB Operation

Fig. 15(a) shows the calculated operation boundary of the hybrid-mode modulation for the converter prototype. At a fixed voltage ratio $d = 0.5$, the output dc current is gradually increased to identify the boundaries of operation modes in both the SAB operation and the proposed hybrid-mode modulation. Fig. 15(b)–(e) shows the operation waveforms of four operation points P1–P4, which correspond to the TR-DCM-Buck mode with $I_{s,dc} = 4$ A, the boundary condition between the TR-DCM-Buck and the TZ-CCM-Buck modes with $I_{s,dc} = 6.7$ A, the TZ-CCM-Buck mode with $I_{s,dc} = 8$ A, and the boundary condition between the TZ-CCM-Buck and the SPS modes with $I_{s,dc} = 9.5$ A, respectively. It is shown that the waveforms of the DAB converter match very well with the SAB converter in different operation modes, where the triangular and trapezoidal transformer current with ZCS turn-OFF of switches are realized. Besides, the natural boundary transitions between the modulation modes are also verified, which coincide with the theoretical analysis. Moreover, it can also be found in Fig. 15(b) that the high-frequency oscillation of v_{CD} in the TR-DCM-Buck mode of the SAB converter is successfully eliminated by the DAB operation. As shown in Fig. 15(f), compared to the SAB operation, the efficiency of the DAB converter with the proposed modulation increases by 2%–2.7% over the whole load range at $d = 0.5$ due to the synchronous rectification.

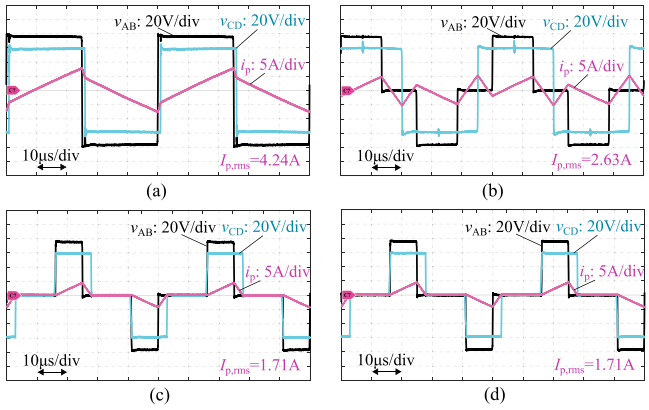

Fig. 16. Measured waveforms at $V_s = 60$ V and $I_{s,dc} = 1$ A. (a) SPS modulation. (b) FOPS modulation [17]. (c) Optimal TPS modulation [24]. (d) Proposed method (TR-DCM-Buck).

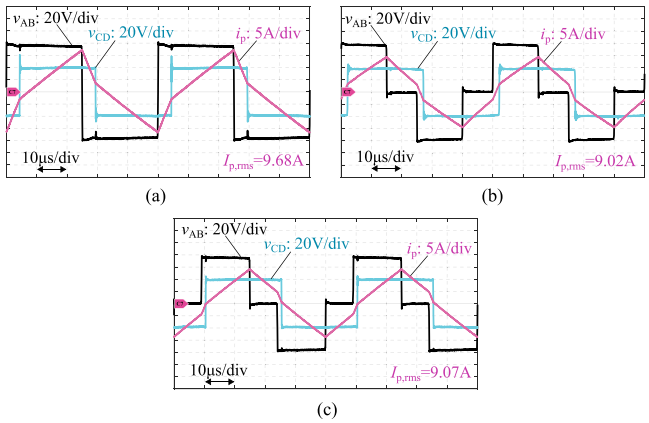

Fig. 17. Measured waveforms at $V_s = 40$ V and $I_{s,dc} = 8$ A. (a) SPS modulation. (b) Optimal TPS modulation [24]. (c) Proposed method (TZ-CCM-Buck).

B. Steady-State Performance

Furthermore, the steady-state performance of the proposed method is compared with the conventional SPS modulation, the FOPS modulation [17] and the optimal TPS modulation [24] under different operation conditions. Fig. 16 shows the operation waveforms at $V_s = 60$ V and $I_{s,dc} = 1$ A, which correspond to the hard-switching operation in the SPS modulation as well as the TR-DCM-Buck mode in the proposed method. Although soft switching can also be realized by the FOPS modulation as depicted in Fig. 16(b), the transformer rms current is obviously larger than the TR-DCM-Buck mode. Moreover, the proposed modulation yields the same switching pattern as the optimal TPS modulation as shown in Fig. 16(c) and (d). Fig. 17 shows the operation waveforms at $V_s = 40$ V and $I_{s,dc} = 8$ A, which corresponds to the TZ-CCM-Buck mode in the proposed method.

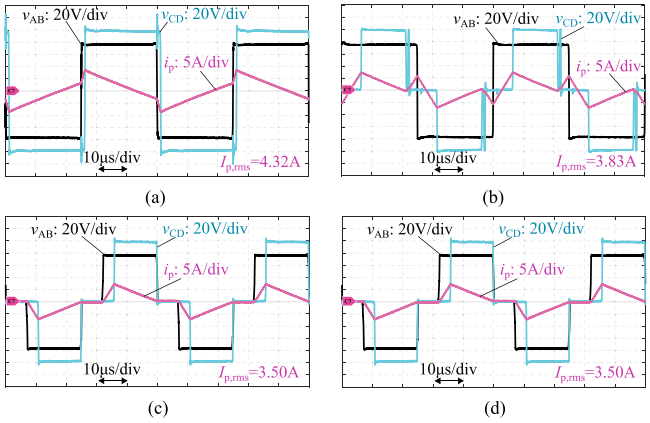

Fig. 18. Measured waveforms at $V_s = 100\,\mathrm{V}$ and $I_{s,dc} = 2\,\mathrm{A}$. (a) SPS modulation. (b) FOPS modulation [17]. (c) Optimal TPS modulation [24]. (c) Proposed method (TR-DCM-Boost).

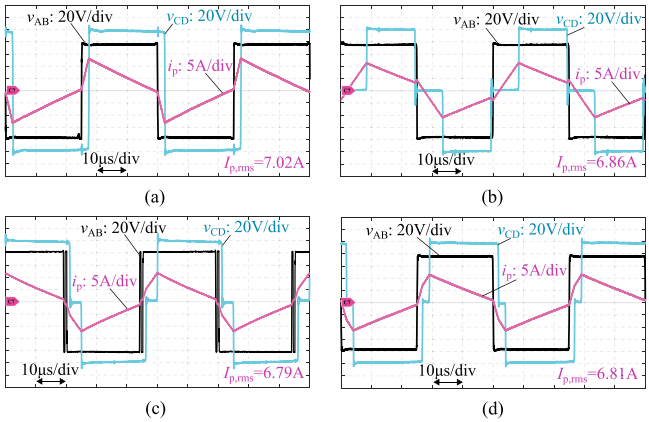

Fig. 19. Measured waveforms at $V_s = 100\,\mathrm{V}$ and $I_{s,dc} = 4.7\,\mathrm{A}$. (a) SPS modulation. (b) FOPS modulation [17]. (c) Optimal TPS modulation [24]. (d) Proposed method (TZ-CCM-Boost).

This operating point is beyond the operation range of the FOPS modulation. It is shown that the optimal TPS modulation and the proposed TZ-CCM-Buck mode can realize ZVS and ZVS/ZCS operation, respectively, with comparable rms currents. Figs. 18 and 19 further show the operation waveforms in the boost mode at $V_s = 100\,\mathrm{V}$ with $I_{s,dc} = 2\,\mathrm{A}$ and $I_{s,dc} = 4.7\,\mathrm{A}$, respectively. In these two cases, both the SPS modulation and FOPS modulation suffer from hard switching. Meanwhile, the DAB converter operates in the TR-DCM-Boost and TZ-CCM-Boost modes in the proposed method, respectively, which realize ZVS/ZCS operation via the triangular or trapezoidal current. From both the optimal TPS modulation and the proposed method, it can be found that the triangular inductor current results in the lowest rms value in the low-power range. Although ZCS turn-OFF can avoid the diode reverse recovery, there is still turn-ON loss due to the charge of the device output capacitance. In practice, the magnetizing current of the transformer can contribute an additional inductive current to assist the charging/discharging process of the output capacitance.

The converter efficiency is also measured and compared among the four modulation methods over a wide operating range. As shown in Fig. 20(a), at $d = 0.5$, the optimal TPS modulation

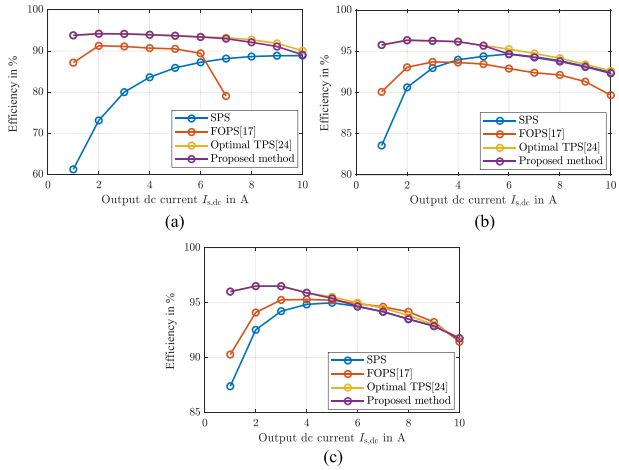

Fig. 20. Measured efficiency curves of the SPS, the FOPS [17], the optimal TPS [24], and the proposed modulation method. (a) $V_s = 40\,\mathrm{V}$, i.e., $d = 0.5$. (b) $V_s = 60\,\mathrm{V}$, i.e., $d = 0.75$. (c) $V_s = 100\,\mathrm{V}$, i.e., $d = 1.25$.

shows the highest efficiency over the whole load range from 1 to 10 A, with the peak value of 94.2% at $I_{s,dc} = 2\,\mathrm{A}$. Compared with the optimal TPS modulation, the proposed method shows a very close performance with the same peak efficiency and a slightly lower efficiency with a difference less than 0.2% in the medium to high load range. Compared with the SPS modulation, the efficiency improvement of the proposed method is up to 30.3%. Besides, the proposed method also achieves a higher efficiency than the FOPS modulation due to the reduced rms current. Similar results are also observed from Fig. 20(b) with $d = 0.75$, which verify the significant efficiency improvements of the proposed method under light-load conditions. It is also found that, with an increasing load current, the efficiency of the SPS modulation becomes even higher than the FOPS modulation due to the reduced rms current. Fig. 20(c) further shows the efficiency curve at $d = 1.25$. In this case, the proposed method and the optimal TPS modulation share the highest light-load efficiency, which is up to 8.6% and 5.7% higher than the SPS modulation and the FOPS modulation, respectively. When the SPS modulation is selected in the proposed method at $I_{s,dc} \geq 5\,\mathrm{A}$, the FOPS modulation shows a slightly improved efficiency with less than 0.5%.

In conclusion, the steady-state performance of the proposed modulation is very close to the optimal TPS modulation [24], which is significantly improved compared to the conventional SPS and the FOPS modulation [17]. However, it should be noticed that the optimal TPS modulation requires a complex optimization algorithm to derive the optimal control parameters, while the proposed method is intuitively derived from the simple SAB operation without any optimization procedure.

C. Load-Transient Performance

The performance of the inherent dynamic control with the proposed hybrid-mode modulation is validated in load-transient tests. In Fig. 21, a step change of the load current from 3 to 9 A occurs at $V_s = 40\,\mathrm{V}$, which results in a smooth transition from the TR-DCM-Buck to the TZ-CCM-Buck mode without a noticeable transient dc-bias current. Meanwhile, ZVS turn-ON

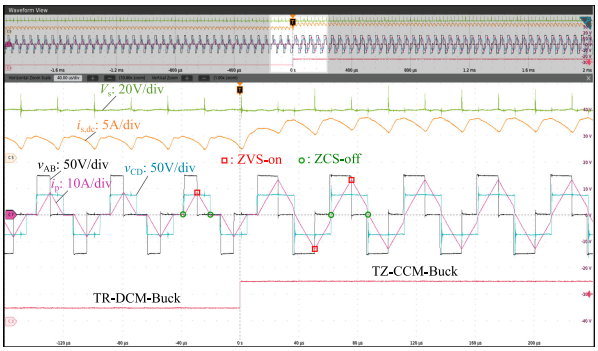

Fig. 21. Measured transient waveforms with the operation-mode change from the TR-DCM-Buck mode with $I_{s,dc} = 3\,A$ to the TZ-CCM-Buck mode with $I_{s,dc} = 9\,A$ at $V_s = 40\,V$.

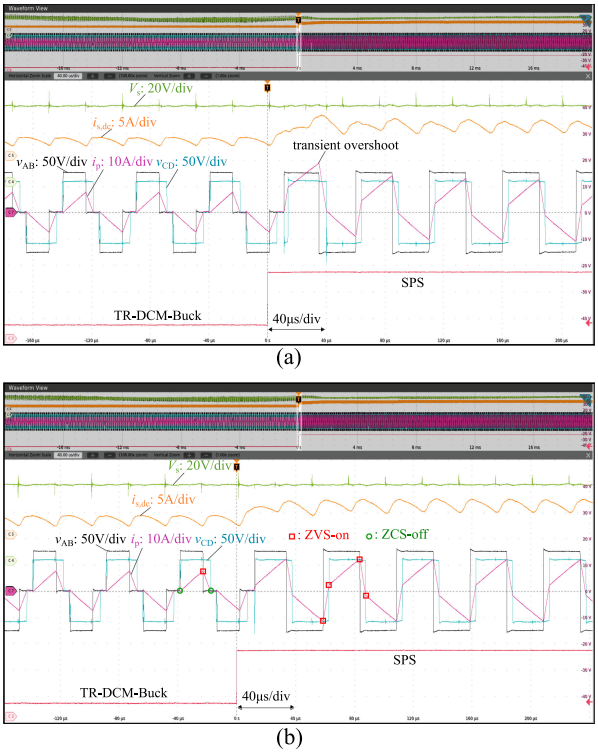

Fig. 22. Measured transient waveforms with the operation-mode change from the TR-DCM-Buck mode with $I_{s,dc} = 3\,A$ to the SPS mode with $I_{s,dc} = 7\,A$ at $V_s = 60\,V$. (a) Conventional SPS modulation. (b) Proposed predictive-current SPS modulation.

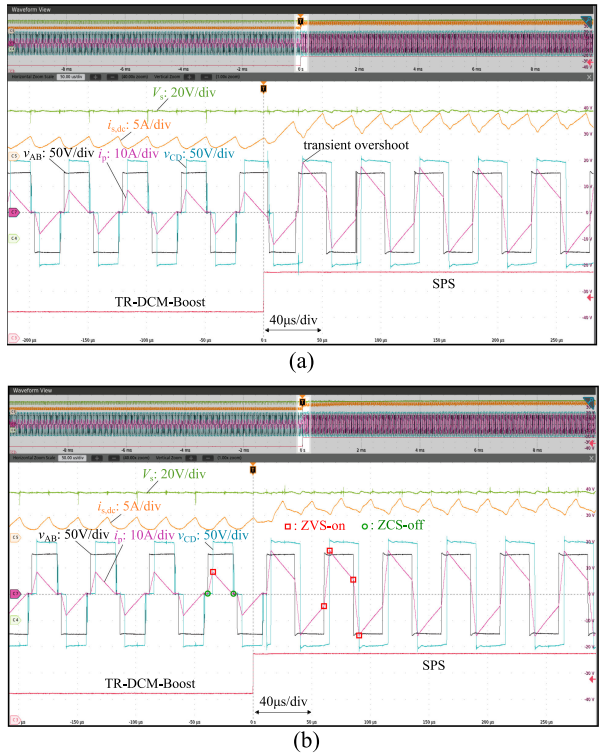

Fig. 23. Measured transient waveforms with the operation-mode change from the TR-DCM-Boost mode with $I_{s,dc} = 3\,A$ to the SPS mode with $I_{s,dc} = 8\,A$ at $V_s = 100\,V$. (a) Conventional SPS modulation. (b) Proposed predictive-current SPS modulation.

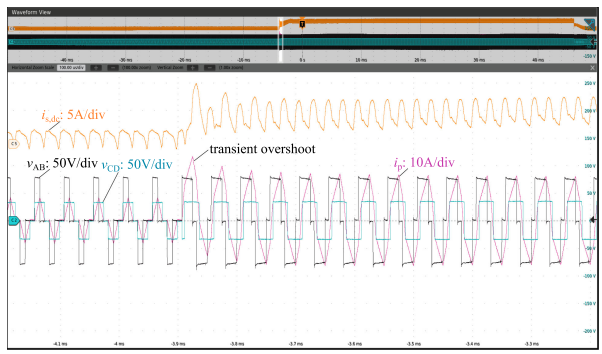

Fig. 24. Measured transient waveforms of the optimal TPS modulation [24] from $I_{s,dc} = 3\,A$ to $I_{s,dc} = 9\,A$ at $V_s = 40\,V$.

and ZCS turn-OFF operation can also be verified in the transient waveforms. Furthermore, Fig. 22 shows a step change of the load current from 3 to 7 A occurs at $V_s = 60\,V$, where the operation mode changes from the TR-DCM-Buck to the SPS mode. Compared with the situation with the conventional SPS modulation as shown in Fig. 22(a), the proposed predictive-current SPS modulation enables a smooth mode transition without a transient dc-bias current as shown in Fig. 22(b). Similar results are observed in Fig. 23, when the load current changes from 3 to 8 A at $V_s = 100\,V$. The operation mode changes from the TR-DCM-Boost to the SPS mode. It is shown that the predictive-current SPS modulation is also effective to avoid a transient dc-bias current in the boost mode. Therefore, it is verified that the proposed hybrid-mode modulation realizes inherent dynamic control with smooth mode transitions under load-transient conditions.

In contrast, a large transient overshoot current is induced under the load transient condition with the optimal TPS modulation [24], as shown in Fig. 24, which takes a few switching cycles to decay.

D. Wide-Range Voltage Control

The proposed hybrid-mode modulation enables an ultrawide-voltage-range operation, which is crucial in many applications

TABLE III
QUALITATIVE COMPARISON OF DIFFERENT MODULATION METHODS

Mode	Number of variables	Soft-sw. range	Type of soft-sw.	RMS current	Optimization complexity	Suppressed transients
SPS [1]	1	Partial	ZVS	Non-optimal	None	No
FOPS [17]	2	Partial (improved)	ZVS	Sub-optimal	Medium	No
Trapezoidal and Triangular modulation [41]	3	Partial (improved)	ZVS/ZCS	Sub-optimal	Low	Yes
Optimal TPS [24]	3	Full	ZVS/ZCS	Optimal	High	No
Proposed method	3	Full	ZVS/ZCS	Sub-optimal	None	Yes

such as black start-up and low-voltage ride through. Fig. 25 shows the transient waveforms of the DAB converter operating in the voltage control mode with the proposed hybrid-mode modulation. As shown in Fig. 25(a), the reference output dc voltage first ramps down from 100 to 10 V with a slope of $-0.3\,\mathrm{V/ms}$, and then, remains constant at 10 V for another 300 ms. Thereafter, the reference output dc voltage ramps up back to 100 V with a slope of $0.3\,\mathrm{V/ms}$. During the whole transient process, the load current remains constant at $I_{\mathrm{s,dc}} = 5.5$ A. It is shown that the output dc voltage is regulated to successfully follow the reference even under the low-voltage-ratio condition, i.e., $d = 0.125$. With the continuously changing operating condition, the operation mode changes smoothly in the sequence of SPS, TZ-CCM-Buck, TR-DCM-Buck, TZ-CCM-Buck, and SPS. Meanwhile, the transformer current is well regulated without an obvious transient overshoot. Moreover, it also verifies that the DAB converter can deliver the same output dc current under the ultralow-voltage condition without increasing the current stress of devices. Fig. 25(b)–(d) further shows the zoomed-in waveforms of the TR-DCM-Buck, TZ-CCM-Buck, and SPS modes, respectively, which validate the effectiveness of the proposed modulation in the voltage control mode.

E. Comparison of Modulation Methods

Based on the previous analysis and experimental validations, the benefits and constraints of the proposed hybrid modulation can be summarized in Table III compared with several state-of-the-art modulation methods. Compared with the SPS, FOPS [17], and conventional trapezoidal and triangular modulation [41], the proposed hybrid modulation and the optimal TPS modulation [24] have more control variables to realize ZVS/ZCS soft switching in the full operating range. Although the optimal TPS modulation [24] results in a globally optimized RMS current, the optimization procedure of control parameters requires complex calculations. In contrast, the proposed modulation is derived intuitively from the SAB operation, which has simple closed-form solutions and does not require any complex optimization process. Moreover, compared with the other modulation methods including the optimal TPS, the proposed modulation can inherently realize smooth mode transitions without transient overshoot currents. This leads to a simple implementation of the closed-loop control with suppressed transients.

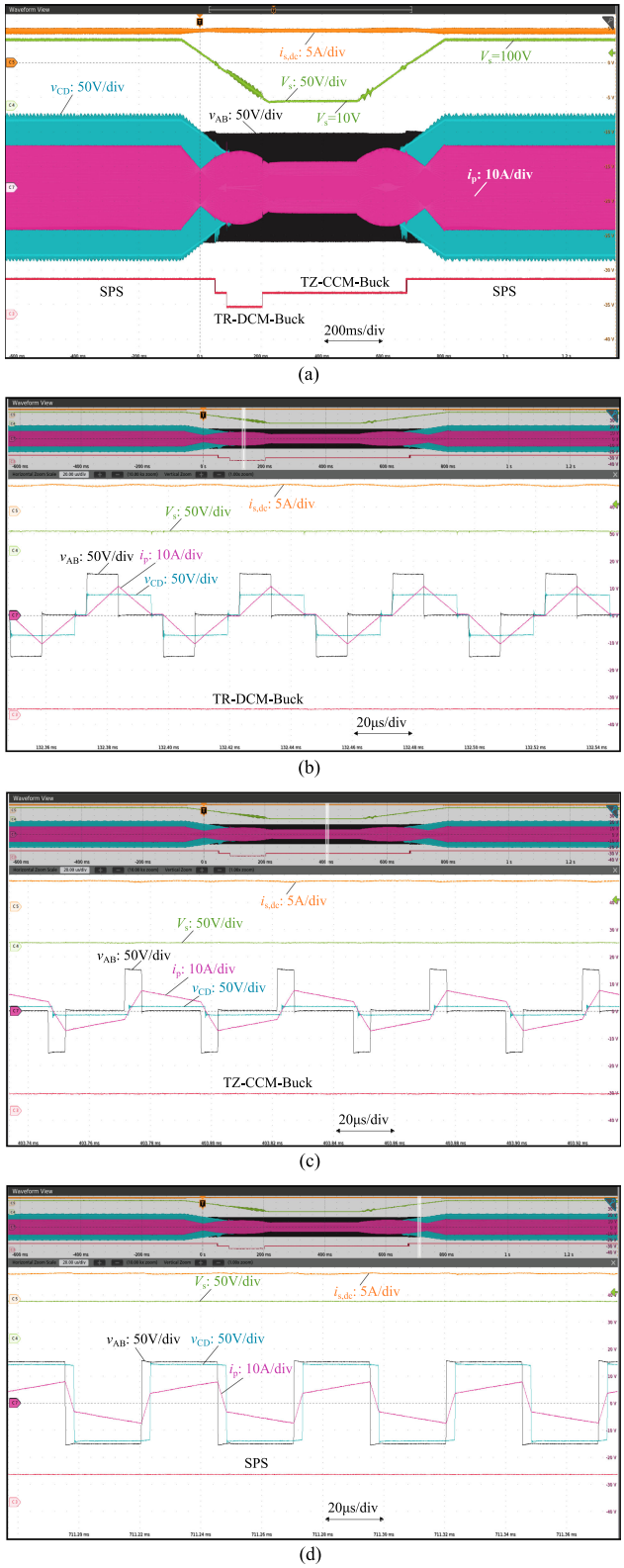

Fig. 25. Measured transient waveforms with ramp changes of the reference output dc voltage from 100 to 10 V at a constant load current of $I_{\mathrm{s,dc}} = 5.5$ A. (a) Whole-process waveforms. (b) Zoomed-in waveforms of the TR-DCM-Buck mode. (c) Zoomed-in waveforms of the TZ-CCM-Buck mode. (d) Zoomed-in waveforms of the predictive-current SPS mode.

V. Conclusion

In this article, a hybrid-mode modulation strategy with natural boundary transitions and inherent dynamic control is proposed for the single-phase DAB converter. Inspired by the quasi-SAB operation, four dedicated modulation modes with the trapezoidal- and triangular current waveforms are intuitively derived, which can naturally and sequentially extend the soft-switching boundary of the SPS modulation to the full operating range with a reduced rms current. Moreover, with the predictive-current SPS modulation, zero initial steady-state transformer current is realized in each of the modulation modes. This enables inherent dynamic control and smooth mode transitions without any dedicated transient-current control strategy. The proposed hybrid-mode modulation with closed-form solutions is implemented in a unified voltage controller, which allows the DAB converter to operate in an ultrawide voltage range with improved overall efficiency and a fast transient response. The effectiveness of the proposed modulation and control methods has been validated by comprehensive experiments on a small-scale DAB converter prototype.

References

[1] R. De Doncker, D. Divan, and M. Kheraluwala, "A three-phase soft-switched high power density DC/DC converter for high power applications," in *Proc. IEEE Ind. Appl. Soc. Annu. Meeting*, 1988, vol. 1, pp. 796–805.

[2] R. W. A. A. De Doncker, D. M. Divan, and M. H. Kheraluwala, "A three-phase soft-switched high-power-density DC/DC converter for high-power applications," *IEEE Trans. Ind. Appl.*, vol. 27, no. 1, pp. 63–73, Jan. 1991.

[3] X. She, A. Q. Huang, and R. Burgos, "Review of solid-state transformer technologies and their application in power distribution systems," *IEEE Trans. Emerg. Sel. Topics Power Electron.*, vol. 1, no. 3, pp. 186–198, Sep. 2013.

[4] J. E. Huber and J. W. Kolar, "Solid-state transformers: On the origins and evolution of key concepts," *IEEE Ind. Electron. Mag.*, vol. 10, no. 3, pp. 19–28, Sep. 2016.

[5] B. Zhao, Q. Song, J. Li, Q. Sun, and W. Liu, "Full-process operation, control, and experiments of modular high-frequency-link DC transformer based on dual active bridge for flexible MVDC distribution: A practical tutorial," *IEEE Trans. Power Electron.*, vol. 32, no. 9, pp. 6751–6766, Sep. 2017.

[6] J. Hu, "Modulation and dynamic control of intelligent dual-active-bridge converter based substations for flexible DC grids," Ph.D. dissertation, Institute for Power Generation and Storage Systems, E.ON Energy Research Center, RWTH Aachen Univ., Aachen, Germany, 2019.

[7] J. Hu, P. Joebges, G. C. Pasupuleti, N. R. Averous, and R. W. De Doncker, "A maximum-output-power-point-tracking-controlled dual-active bridge converter for photovoltaic energy integration into MVDC grids," *IEEE Trans. Energy Convers.*, vol. 34, no. 1, pp. 170–180, Mar. 2019.

[8] T. Liu *et al.*, "Design and implementation of high efficiency control scheme of dual active bridge based 10 kV/1 MW solid state transformer for PV application," *IEEE Trans. Power Electron.*, vol. 34, no. 5, pp. 4223–4238, May 2019.

[9] S. Inoue and H. Akagi, "A bidirectional DC-DC converter for an energy storage system with galvanic isolation," *IEEE Trans. Power Electron.*, vol. 22, no. 6, pp. 2299–2306, Nov. 2007.

[10] R. Xie and H. Li, "Fault performance comparison study of a dual active bridge (DAB) converter and an isolated modular multilevel DC/DC (iM2DC) converter for power conversion module application in a breakerless shipboard MVDC system," *IEEE Trans. Ind. Appl.*, vol. 54, no. 5, pp. 5444–5455, Sep./Oct. 2018.

[11] G. Buticchi, D. Barater, L. F. Costa, and M. Liserre, "A PV-inspired low-common-mode dual-active-bridge converter for aerospace applications," *IEEE Trans. Power Electron.*, vol. 33, no. 12, pp. 10 467–10 477, Dec. 2018.

[12] N. H. Baars, J. Everts, H. Huisman, J. L. Duarte, and E. A. Lomonova, "A 80-kW isolated DC-DC converter for railway applications," *IEEE Trans. Power Electron.*, vol. 30, no. 12, pp. 6639–6647, Dec. 2015.

[13] F. An, W. Song, K. Yang, S. Yang, and L. Ma, "A simple power estimation with triple phase-shift control for the output parallel DAB DC-DC converters in power electronic traction transformer for railway locomotive application," *IEEE Trans. Transp. Electrific.*, vol. 5, no. 1, pp. 299–310, Mar. 2019.

[14] N. Hou and Y. W. Li, "Overview and comparison of modulation and control strategies for a nonresonant single-phase dual-active-bridge DC-DC converter," *IEEE Trans. Power Electron.*, vol. 35, no. 3, pp. 3148–3172, Mar. 2020.

[15] G. G. Oggier, R. Leidhold, G. O. Garcia, A. R. Oliva, J. C. Balda, and F. Barlow, "Extending the ZVS operating range of dual active bridge high-power DC-DC converters," in *Proc. 37th IEEE Power Electron. Spec. Conf.*, Jun. 2006, pp. 1–7.

[16] G. Oggier, G. O. García, and A. R. Oliva, "Modulation strategy to operate the dual active bridge DC-DC converter under soft switching in the whole operating range," *IEEE Trans. Power Electron.*, vol. 26, no. 4, pp. 1228–1236, Apr. 2011.

[17] B. Zhao, Q. Song, W. Liu, G. Liu, and Y. Zhao, "Universal high-frequency-link characterization and practical fundamental-optimal strategy for dual-active-bridge DC-DC converter under PWM plus phase-shift control," *IEEE Trans. Power Electron.*, vol. 30, no. 12, pp. 6488–6494, Dec. 2015.

[18] H. Bai and C. Mi, "Eliminate reactive power and increase system efficiency of isolated bidirectional dual-active-bridge DC-DC converters using novel dual-phase-shift control," *IEEE Trans. Power Electron.*, vol. 23, no. 6, pp. 2905–2914, Nov. 2008.

[19] N. Schibli, "Symmetrical multilevel converters with two quadrant DC-DC feeding," Ph.D. dissertation, Industrial Electronics Laboratory, Swiss Federal Institute of Technology Lausanne (EPFL), Lausanne, Switzerland, 2000.

[20] F. Krismer and J. W. Kolar, "Accurate small-signal model for the digital control of an automotive bidirectional dual active bridge," *IEEE Trans. Power Electron.*, vol. 24, no. 12, pp. 2756–2768, Dec. 2009.

[21] J. Huang, Y. Wang, Z. Li, and W. Lei, "Unified triple-phase-shift control to minimize current stress and achieve full soft-switching of isolated bidirectional DC-DC converter," *IEEE Trans. Ind. Electron.*, vol. 63, no. 7, pp. 4169–4179, Jul. 2016.

[22] F. Krismer and J. W. Kolar, "Closed form solution for minimum conduction loss modulation of DAB converters," *IEEE Trans. Power Electron.*, vol. 27, no. 1, pp. 174–188, Jan. 2012.

[23] N. Hou, W. Song, and M. Wu, "Minimum-current-stress scheme of dual active bridge DC-DC converter with unified phase-shift control," *IEEE Trans. Power Electron.*, vol. 31, no. 12, pp. 8552–8561, Dec. 2016.

[24] A. Tong, L. Hang, G. Li, X. Jiang, and S. Gao, "Modeling and analysis of a dual-active-bridge-isolated bidirectional DC/DC converter to minimize RMS current with whole operating range," *IEEE Trans. Power Electron.*, vol. 33, no. 6, pp. 5302–5316, Jun. 2018.

[25] S. Shao, M. Jiang, W. Ye, Y. Li, J. Zhang, and K. Sheng, "Optimal phase-shift control to minimize reactive power for a dual active bridge DC-DC converter," *IEEE Trans. Power Electron.*, vol. 34, no. 10, pp. 10193–10205, Oct. 2019.

[26] J. Hu, S. Cui, D. V. D. Hoff, and R. W. De Doncker, "Generic dynamic phase-shift control for bidirectional dual-active bridge converters," *IEEE Trans. Power Electron.*, vol. 36, no. 6, pp. 6197–6202, Jun. 2021.

[27] Q. Bu, H. Wen, J. Wen, Y. Hu, and Y. Du, "Transient DC bias elimination of dual-active-bridge DC-DC converter with improved triple-phase-shift control," *IEEE Trans. Ind. Electron.*, vol. 67, no. 10, pp. 8587–8598, Oct. 2020.

[28] J. Hu, S. Cui, S. Wang, and R. W. De Doncker, "Instantaneous flux and current control for a three-phase dual-active bridge DC-DC converter," *IEEE Trans. Power Electron.*, vol. 35, no. 2, pp. 2184–2195, Feb. 2020.

[29] S. Wang, C. Li, K. Wang, Z. Zheng, and Y. Li, "Loss imbalance and transient DC-bias mitigation in dual active bridge DC/DC converters," *IEEE Trans. Emerg. Sel. Topics Power Electron.*, vol. 9, no. 2, pp. 1399–1409, Apr. 2021.

[30] B. Zhang, S. Shao, L. Chen, X. Wu, and J. Zhang, "Steady state and transient DC magnetic flux bias suppression methods for a dual active bridge converter," *IEEE Trans. Emerg. Sel. Topics Power Electron.*, vol. 9, no. 1, pp. 744–753, Feb. 2021.

[31] W. Li, S. Zong, F. Liu, H. Yang, X. He, and B. Wu, "Secondary-side phase-shift-controlled ZVS DC/DC converter with wide voltage gain for high input voltage applications," *IEEE Trans. Power Electron.*, vol. 28, no. 11, pp. 5128–5139, Nov. 2013.

[32] H. Wu, Y. Lu, T. Mu, and Y. Xing, "A family of soft-switching DC-DC converters based on a phase-shift-controlled active boost rectifier," *IEEE Trans. Power Electron.*, vol. 30, no. 2, pp. 657–667, Feb. 2015.
[33] D. Sha, J. Zhang, and Y. Xu, "Improved boundary operation for voltage-fed semi-DAB with ZVS achievement and nonactive power reduction," *IEEE Trans. Ind. Electron.*, vol. 64, no. 8, pp. 6179–6189, Aug. 2017.
[34] R. U. Lenke, J. Hu, and R. W. De Doncker, "Unified steady-state description of phase-shift-controlled ZVS-operated series-resonant and non-resonant single-active-bridge converters," in *Proc. IEEE Energy Convers. Congr. Expo.*, 2009, pp. 796–803.
[35] K. Park and Z. Chen, "Analysis and design of a parallel-connected single active bridge DC-DC converter for high-power wind farm applications," in *Proc. 15th Eur. Conf. Power Electron. Appl.*, 2013, pp. 1–10.
[36] Y. Sang, A. Junyent-Ferré, and T. C. Green, "Operational principles of three-phase single active bridge DC/DC converters under duty cycle control," *IEEE Trans. Power Electron.*, vol. 35, no. 8, pp. 8737–8750, Aug. 2020.
[37] N. Hou, W. Song, Y. Li, Y. Zhu, and Y. Zhu, "A comprehensive optimization control of dual-active-bridge DC-DC converters based on unified-phase-shift and power-balancing scheme," *IEEE Trans. Power Electron.*, vol. 34, no. 1, pp. 826–839, Jan. 2019.
[38] Z. Guo, Y. Luo, and K. Sun, "Parameter identification of the series inductance in DAB converters," *IEEE Trans. Power Electron.*, vol. 36, no. 7, pp. 7395–7399, Jul. 2021.
[39] J. Hu, Z. Yang, S. Cui, and R. W. De Doncker, "Closed-form asymmetrical duty-cycle control to extend the soft-switching range of three-phase dual-active-bridge converters," *IEEE Trans. Power Electron.*, vol. 36, no. 8, pp. 9609–9622, Aug. 2021.
[40] J. Everts, F. Krismer, J. van den Keybus, J. Driesen, and J. W. Kolar, "Optimal ZVS modulation of single-phase single-stage bidirectional DAB AC-DC converters," *IEEE Trans. Power Electron.*, vol. 29, no. 8, pp. 3954–3970, Aug. 2014.
[41] D. Goldmann, S. Schramm, and H.-G. Herzog, "Triangular and trapezoidal modulation for dual active bridge DC-DC converters with fast switching semiconductors," in *Proc. 21st Eur. Conf. Power Electron. Appl.*, 2019, pp. P.1–P.10.

Jingxin Hu (Member, IEEE) received the B.S. degree from Northeastern University, Shenyang, China, in 2010, and the M.Sc. and Dr.-Ing. degrees, with the highest distinction (*summa cum laude*), from RWTH Aachen University, Aachen, Germany, in 2013 and 2019, respectively, all in electrical engineering.

From April 2012 to October 2012, he was a Research Intern with ABB Corporate Research Center, Baden-Dättwil, Switzerland. In 2013, he joined General Electric Global Research Center, Munich, Germany. Since October 2014, he has been with the Institute for Power Generation and Storage Systems, E.ON Energy Research Center, RWTH Aachen University, where he is currently a Senior Scientist. Since February 2021, he has also been the Research Project Leader with FEN GmbH, Germany. His research interests include power electronics, solid-state transformers, medium-voltage dc and low-voltage dc distribution systems, and applications of wide-bandgap devices.

Dr. Hu was the recipient of the RWTH Aachen—University of Alberta Senior Research Fellowship in 2021, the STAWAG Best Dissertation Prize of RWTH Aachen University in 2019, the Chinese Government Award for Outstanding Self-Financed Students Abroad in 2019, and the Second Prize Paper Award of IEEE International Power Electronics Conference (ECCE Asia) in 2018.

Shenghui Cui (Member, IEEE) received the B.S. degree from Tsinghua University, Beijing, China, in 2012, the M.S. degree from Seoul National University, Seoul, South Korea, in 2014, and the Dr.-Ing. degree with the highest distinction (*summa cum laude*) from RWTH Aachen University, Aachen, Germany, in 2019, all in electrical engineering.

Since September 2021, he has been with the Department of Electrical and Computer Engineering, Seoul National University, as an Assistant Professor. From March 2015 to May 2021, he was with the Institute for Power Generation and Storage Systems, E.ON Energy Research Center, RWTH Aachen University, where he worked as a Research Associate and later on as a Senior Scientist. His research interests include interaction of power systems and power converters, power converters in ac/dc utility applications, and applications of wide-band gap power devices.

Dr. Cui was the recipient of the STAWAG Best Dissertation Prize from the Faculty of Electrical Engineering and Information Technology, RWTH Aachen University, in 2019, the Second Place Prize Paper Award of the IEEE TRANSACTIONS ON POWER ELECTRONICS in 2018, the Second Prize Paper Award of IEEE International Power Electronics Conference (ECCE Asia) in 2018, and the Outstanding Presentation Award of the IEEE Applied Power Electronics Conference in 2014.

Rik W. De Doncker (Fellow, IEEE) received the Ph.D. degree in electrical engineering from Katholieke Universiteit Leuven, Leuven, Belgium, in 1986.

In 1987, he was a Visiting Associate Professor with the University of Wisconsin-Madison, Madison, WI, USA, in 1988, a Senior Scientist with GE CR&D, Schenectady, NY, USA, in 1994, Vice President Technology of SPCO, developing world's first medium-voltage static transfer switches. Since October 1996, he has been a Professor with RWTH Aachen University, Aachen, Germany, leading the Institute for Power Electronics and Electrical Drives. In 2006, he became the Director with E.ON ERC, RWTH and founded the Institute for Power Generation and Storage Systems. He leads the RWTH CAMPUS Cluster Sustainable Energy and the BMBF Flexible Electrical Networks Research CAMPUS. Since 2010, he has been a member of the German National Platform for Electric Mobility, since 2017, of the French VEDECOM, and since 2016, of the German Academy of Science and Technology.

Dr. Doncker was the recipient of the IEEE Industry Applications Society Outstanding Achievements Award, the Power and Energy Society Nari Hingorani Custom Power Award in 2008, the 2013 Newell Power Electronics Field Award, the 2014 IEEE IEEE Power Electronics Society H. Owen Outstanding Service Award, RWTH Fellow status in 2015, and the IEEE Gold Medal in Power Engineering in 2020.